Modeling and Control Techniques for Landing on (99942) Apophis: An Analysis of a Mission Scenario

Victor Hernandez Megia[a,*], Tra-Mi Ho[a], Jan Thimo Grundmann[a], Matthias Noeker[b]

[a] *German Aerospace Center (DLR), Institute of Space Systems, Bremen, 28359, Germany*
[b] *German Space Agency at DLR, Bonn, 53227, Germany*

Abstract

On April 13 2029, the near-Earth asteroid (99942) Apophis will perform a close flyby within a distance of 32,000 km of Earth's surface. This event, which is 10 times closer than the Moon and closer than many geostationary communication satellites, offers an unprecedented opportunity to study an asteroid in great detail. To leverage this close encounter, a fast sample return mission, APOSSUM, was designed using ESA's current RAMSES mission as a use case. This paper presents a detailed analysis of the APOSSUM mission scenario, focusing on feasibility. It covers the separation of the APOSSUM probe, its cruise toward Apophis, and the subsequent landing and return phases. Particular emphasis is placed on the landing scenario, with studies of different density models of Apophis and a comparison of control techniques for precision landing. The findings from this mission will significantly advance understanding of small-body landing maneuvers.

Keywords: Asteroid landing, Apophis mission, Spacecraft guidance and control, Gravitational modeling, Sample return missions

Nomenclature

ΔV**:** Change in velocity
AEM: Asteroid Exploration Mission
APOSSUM: APOphiS SUrfaces saMpler
AU: Astronomical Unit
CE: Concurrent Engineering
CM: Center of Mass
DART: Double Asteroid Redirect Test
DLR: German Aerospace Center
ESA: European Space Agency
FPA: Flight Path Angle
G: Gravitational Constant
GM: Standard Gravitational Parameter
GNC: Guidance, Navigation, and Control
HERA: ESA Planetary Defense Mission
JAXA: Japan Aerospace Exploration Agency
LEO: Low Earth Orbit
NASA: National Aeronautics and Space Administration
NEO: Near-Earth Object
PD: Proportional-Derivative Control
RAMSES: Rapid Apophis Mission for Space Safety
RK45: Runge-Kutta Method (Order 4-5)
SPH: Spherical Harmonics
SRP: Solar Radiation Pressure
STK: Systems Tool Kit (Ansys Software)
T: Thrust
TC: Telecommands
V: Gravitational Potential

[⋆] This research was carried out at the German Aerospace Center (DLR).

[*] Corresponding author. Email: victor.legazpi@gmail.com; ORCID: 0009-0000-8282-6022

https://doi.org/10.1016/j.actaastro.2025.04.31

1. Introduction

Asteroids are essential for understanding the solar system from its emerging stages. They are remains of early solar system stages and give valuable clues about the basic building blocks that made up a planet or other objects in the solar system. Asteroids are like time capsules, as they hold conditions from 4.5 billion years ago [1]. Most asteroids are located in the Main Belt and the Kuiper Belt.

In the recent past years they have gained significant relevance in the scientific community driven by the information these objects hide in their (sub-) surfaces to understand the building blocks of planets. This information includes not only their composition and formation processes but also potential clues about the origins of life on Earth, as some essential elements for life may have been given by asteroids [2]. This theory is supported by the results of JAXA's Hayabusa2 mission to asteroid Ryugu [3], [4] and NASA's OSIRIS-REx to asteroid Bennu [5], [6].

Furthermore, studying asteroids can help develop strategies to change their trajectories, thus preventing potential collisions with Earth [7]. The current double mission for planetary defense, DART (Double Asteroid Redirect Test) of NASA [8] and HERA of ESA [9] have these objectives. The DART spacecraft has successfully impacted on Didimorphos, the moonlet of the asteroid binary system Didymos, and was able to change its trajectory setting a step towards a future in which humans are able to deviate asteroids and avoid collisions [10].

ESA is currently planning a direct successor mission to Hera, the RAMSES mission [11] to be launched in 2028 targeting the near-Earth asteroid (99942) Apophis. This asteroid will encounter Earth in 2029, passing at a distance closer than geostationary orbit at its closest point (= 32,000 km). In this context, the Max Planck Institute for Solar System Research (MPS), together with the German Aerospace Centre (DLR) and the University of Münster, conducted a study on returning asteroid samples from Apophis, the APOphiS SUrfaces saMpler (APOSSUM), using the extremely short return distance to Earth [12]. ESA's RAMSES mission was used in the study as a mission-architectural use case, i.e. the APOSSUM probe should be launched piggybacked with RAMSES as the carrier spacecraft. Thus, all components were adapted to the launcher and to RAMSES to perform the sample recollection and return. In addition to expanding the existing dataset of extraterrestrial materials captured in-situ such as from the Hayabusa, the Hayabusa2 [4] and the OSIRIS-REx missions [6], and thereby increasing our scientific knowledge of asteroids, APOSSUM also aims to explore new technological frontiers in spacecraft navigation, guidance and landing techniques [13].

Previous studies have investigated the dynamics and operation of a spacecraft in the proximity of an asteroid [14]. In this paper we will will present different landing scenarios of the APOSSUM probe on Apophis by taking into account two different density scenarios for the asteroid. There are different methods to model the gravitation around an asteroid based on its density distributions. [15] for example employ finite element methods to estimate internal density variations and gravitational fields of small bodies. This study utilizes spherical harmonics and the tetrahedral approach to model Apophis's gravitational potential, specifically to optimize landing maneuvers and develop control techniques tailored to the APOSSUM mission.

2. APOSSUM Mission Overview

The main mission goal of APOSSUM is collecting samples from Apophis' surface and bring them back to Earth. The mission is divided in 3 distinct phases. The first one ("Separation and Approach") deals with the detachment of the APOSSUM probe from the RAMSES spacecraft at a distance of 20 km from Apophis and its flight to the asteroid up to a distance of 1 km. This phase was studied using spherical harmonics and a constant density for the model of Apophis. As will be discussed in further sections, it is a good approximation since the size is insufficient to cause relevant perturbations at those great distances. The results will be presented in the later sections.

The second phase ("landing") covers approaching the asteroid from 1 km above the surface to a target point. For this paper, the target point was selected randomly since there are currently no detailed information on the composition of Apophis' surface for dedicated sampling and therefore a random location is used to investigate the control techniques and scenario. This is in accordance with the mission and scientific requirement of APOSSUM that the landing spot will be selected upon arrival. Building upon the orbital dynamic models discussed in [14], our analysis incorporates those perturbations in the landing model but extending them using other shape and density. As Apophis's density and shape are critical to the final approach phase, as outlined in [16], [17], we have analyzed several scenarios to determine the variability of the final approach phase and draw conclusions for navigation during this phase. For this phase, we used Python (specifically using the following libraries :open3d, to open the asteroid model and load the mesh, numpy, for the computations and matplotlib.pyplot, to have a plot style similar to MATLAB [18]) and all the solutions were derived through numerical methods. Different approaches are simulated and compared to provide a detailed assessment of their viability and performance.

Finally, a third phase ("Earth Return") is shown, it involves the return of the APOSSUM lander to a designated landing location on Earth. In this phase, STK is used, assuming an ellipsoid of constant density, since the time it stays in the sphere of influence is short and the main perturbations come from SRP (Solar Radiation Pressure), Luni-solar gravitational effects, and nonsphericity of Earth. The APOSSUM lander will depart from the surface of the asteroid and land in Woomera (Australia),this is exemplary landing location for this study, similar to the return of the Hayabusa2 samples [4], The landing location was selected because APOSSUM would land on the opposite side of Earth relative to Apophis during the closest approach. This requirement allows telescopes in other parts of the world to continuously monitor the trajectory of the Apophis asteroid and study it during the closest approach.

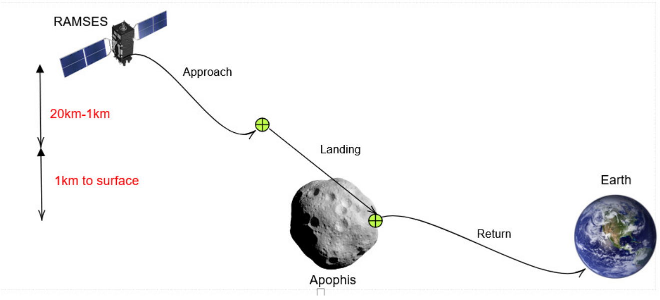

Figure 1: APOSSUM mission scenario. The figure illustrates all three phases as described in the document. Note that it is not to scale and uses a generic asteroid image to represent Apophis.

Figure 1 illustrates all three phases as described above. It should be noted that it is not to scale. Furthermore, it has been created with a generic asteroid image representing the asteroid.

3. Model Used and its characteristics

Operations at close range, especially when touching or landing on an asteroid's surface depend strongly on the gravity field of the target object. Most dynamic analyses of the approach to an asteroid primarily use spherical harmonics or ellipsoidal harmonics to model the gravity of this small body, as described in the previous section. However, once the operation passes the circumscribing sphere (Brillouin sphere) [15], i.e. in the case of touching the asteroid for sampling, the gravitational field will diverge due to the irregular shape and varying density distribution of the asteroid.
For our analysis of landing maneuvers, we have used the Apophis data obtained by NASA radar observations in 2013 which led to the tetrahedral shape used of the asteroid [19] and [20], as presented in Figure 2.

We have chosen this method for modelling the shape of the asteroid, taking into account that there is no case studied in which that amount of vertex and shapes are found to represent Apophis shape. However, this shape model allows us to include different densities and to investigate the dependence of the approach and landing manoeuvres of the APOSSUM probe.

The shape model of Apophis [21] was re-constructed using MeshLab, an open-source, purpose-built tool for processing and editing unstructured 3D triangular meshes to enable detailed simulation and analysis [22]. The first step was rescaling the reconstructed model in line with the asteroid's known physical dimensions, see Table 1, so the simulations would be in line with real-case scenarios for the APOSSUM mission. This rescaled mesh serves as the foundational geometric model for further gravitational and landing dynamics simulations. For the bulk density

Variable	**Value [m]**
x axis	450
y axis	370
z axis	170

Table 1: Dimensions of the asteroid Apophis [23]

of Apophis, we have adopted for our simulation densities between 1.29 - 3.5 g/cm^3 based on the assessment of [16]. To model the interaction of the APOSSUM probe with the asteroid, we will use different density models. For the "Separation and Approach" phase, we will assume that Apophis has a constant density. For the landing phase, we will model Apophis with varying density distribution since gravitational attraction will diverge within the Brillouin sphere and therefore its influence on the close approach and landing trajectory, finally for the return phase, the asteroid will be approximated as an ellipsoid with constant density and the main perturbations will come from the lunisolar gravitational attraction, SRP and the non-sphericity of Earth.

The trajectories in this manuscript are generated in an asteroid-fixed coordinate system. This choice allows for accurate modeling of the gravitational field, rotational dynamics, and the relative motion of the lander with respect to Apophis. The asteroid-fixed system is essential for simulations involving trajectory corrections and landing maneuvers, as it captures the local gravitational and rotational effects that influence the spacecraft's approach and stability during touchdown.

4. Phase 1: Separation and Approach to Apophis

As mentioned in section 2, the APOSSUM probe will be separated from the RAMSES spacecraft at a 20 km distance. As explained for this phase, we used Spherical Harmonics for trajectory determination and described the gravitational field of Apophis, assuming a bulk density of roughly 3.2 g/cm^3 which corresponds to a mass of $6.1 \cdot 10^{10}$ kg. For this first phase and due to the order of magnitude of the distances towards the asteroid, SPH is more suitable because it is more efficient and the detail given by the alternative method used in this study (tetrahedral method) is not needed. Surely, given its size and properties, it is unlikely that Apophis is composed of a single composition, and thus a constant density.

4.1. Spherical Harmonics for Gravitational Field Representation

The spherical harmonics are composed of series of orthogonal functions defined on the surface of the sphere

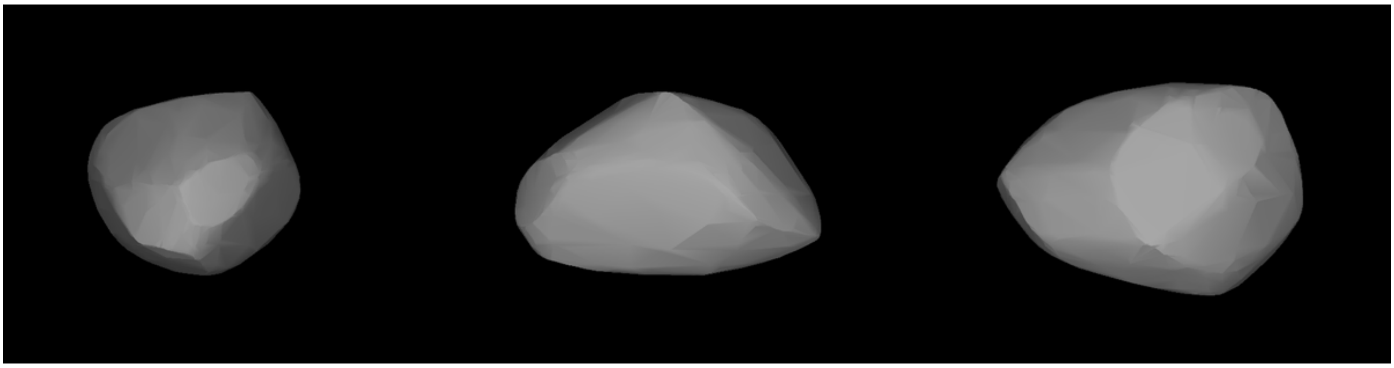

Figure 2: Apophis shape of the tetrahedral model [19] [20]

to solve problems which involve Laplace´s equations in Spherical coordinates. They are used to compute the imperfections of an object and to model it. This approach is convenient from the computational point of view but also from the analytical one since they are able to provide results in a short period of time, while keeping the accuracy in them [24].

$$Y_n^m(\theta,\phi) = \sqrt{\frac{(2n+1)(n-m)!}{4\pi(n+m)!}} P_n^m(\cos\theta) e^{im\phi}$$

Here, P_n^m are the associated Legendre polynomials, and $e^{im\phi}$ represents the complex exponential function, essential for incorporating azimuthal symmetry [24].

$$V(r,\theta,\phi) = -\frac{GM}{r}\left(1 + \sum_{n=1}^{\infty}\left(\frac{R}{r}\right)^n \sum_{m=0}^{n} P_n^m(\cos\theta) \cdot (C_{nm}\cos m\phi + S_{nm}\sin m\phi)\right) \quad (1)$$

where:

- r is the radial distance,
- θ and ϕ are the polar and azimuthal angles, respectively,
- G is the gravitational constant,
- M is the total mass of the object,
- R is the reference radius of the object which is 185m [16],
- C_{nm}, S_{nm} are the coefficients of the spherical harmonic terms,
- $Y_n^m(\theta,\phi)$ are the spherical harmonic functions

Thus, the real and imaginary coefficients for the harmonic terms are computed as follows:

$$C_{nm} = \sum_i \text{Area}_i \cdot \text{Re}(Y_n^m(\theta_i,\phi_i)) \quad (2)$$

$$S_{nm} = \sum_i \text{Area}_i \cdot \text{Im}(Y_n^m(\theta_i,\phi_i)) \quad (3)$$

Using above formulas applied to the model, the following potentials are obtained.

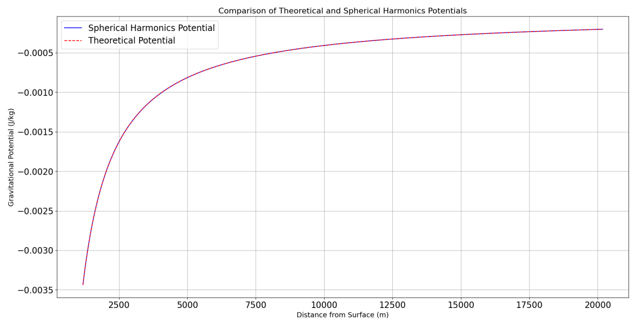

Figure 3: The calculated potential between 1 km to 20 km distance to Apophis, theoretically and with SPH. The X-axis represents the distance from the surface in meters and the Y-axis the gravitational potential in J/kg

The resulting potential is nearly constant, and its value is very close to the theoretical one given by $-\frac{GM}{r}$ [25] as shown in Figure 3. The resultant mass is 6.1 $\cdot 10^{10}$ kg which corresponds to the density value of 3.2 g/cm^3 (i.e. worst-case scenario, since it is the upper bound of the expected density), both values within the expected range of the asteroid [16]. Additionally, it is noteworthy that the potential is really constant; this is such because the location of the center of mass is shifted just few meters from the origin.

Once the potential is well known, the computation of the trajectory can be obtained. The force is computed knowing that F= $-\frac{dU}{dr}$ [25]. With that in mind, a dynamic function is created, and using the Runge-Kutta 45 method, the trajectory is computed [26].

To include this influence of SRP, the current designed mass of APOSSUM of approximately 100 kg and the cross-sectional area is 0.2205 m^2 is used as input [13]. (In this case, the worst scenario possible was used, and so the spacecraft is always facing the Sun in such a way that the area is maximum).

The SRP formula is computed assuming that the distance from Apophis to the Sun is 1 AU and constant [27]. This is a good approximation since the variation is minimum as shown in [28].

$$\mathbf{a}_{\text{SRP}} = \frac{P_{\text{SRP}} \cdot A_{\text{SRP}}}{m_{\text{sc}}} \hat{\mathbf{s}} \tag{4}$$

where:

- $\vec{a}_{\text{SRP}}$ is the acceleration due to solar radiation pressure,
- P_{SRP} is the solar radiation pressure at 1 AU (Astronomical Unit) in N/m^2,
- A_{SRP} is the cross-sectional area of the spacecraft affected by the solar radiation in m^2,
- m_{sc} is the mass of the spacecraft in kg,
- $\hat{s}$ is the unit vector from the spacecraft towards the Sun, assuming the Sun's influence is along the positive x-axis.

In addition, the direction of the pressure was along the x-axis, this is such since it has to be the worst-case scenario and the position of release from RAMSES [11] is still unknown and Apophis is a tumbling rotator. This means that the orientation of the spacecraft with respect to the asteroid and to the SUN is undefined and therefore, the calculations are done to have a conservative result.

With all those factors considered and included in the dynamics function, the trajectory is computed again with the same initial conditions as before. This is shown in Figure 4

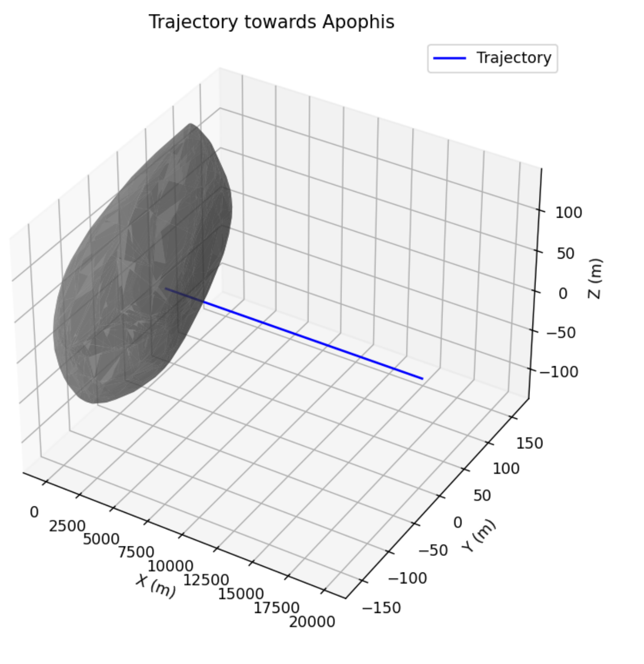

Figure 4: Trajectory to approach Apophis with solar radiation pressure (SRP) applied. The trajectory showcases the spacecraft's path under the influence of SRP.

The ΔV required to accomplish this maneuver was 1.6 m/s and was achieved over a span of 2.7 hours. This ΔV can be adjusted to achieve a more fuel-efficient approach by increasing the time required.

Moreover, it can be seen that at these distances and for a first approach, the lander just need one impulse upon arrival and the control technique is still not needed.

5. Phase 2: Landing on Apophis

In this section, the landing maneuvers and scenario will be studied in detail. This phase begins when the APOSSUM spacecraft reaches a distance of 1 km from the surface. A couple of density scenarios are analyzed and ultimately one is selected as the most plausible for the mission.

For this part, we used the tetrahedral method because of the accuracy it brings and the suitability to incorporate several densities in the model. Moreover, according to [29], SPH may produce divergence when computing the trajectories due to the fact that APOSSUM enters the Brillouin sphere.

5.1. Mesh Processing and Area Calculation

In order to use tetrahedral technique for modeling, the imported mesh of the model is processed to compute key geometric parameters, such as surface area and volume, which are essential for distributing densities accurately across the model.
The model is imported to the code, and the geometric properties of it are computed. These calculations are performed using Heron's formula [30] for all the triangular facets of the mesh, since it is crucial for an accurate distribution of mass over the asteroid's surface.

$$a = \|\mathbf{v}_2 - \mathbf{v}_1\|, \quad b = \|\mathbf{v}_3 - \mathbf{v}_2\|, \quad c = \|\mathbf{v}_1 - \mathbf{v}_3\| \tag{5}$$

$$s = \frac{a+b+c}{2} \tag{6}$$

$$Area = \sqrt{s(s-a)(s-b)(s-c)} \tag{7}$$

5.2. Tetrahedral method and gravitational potential

To compute the trajectories in detail, the whole volume of the model is divided in tetrahedral elements [17] using 3 vertices and one middle point chosen to be in the center of the asteroid. The mass is then computed by the formula:

$$m = \rho \cdot V \tag{8}$$

Where V is the volume of the tetrahedral used in that iteration and ρ the density. The mass is divided in those 3 vertices chosen and the process is repeated for the whole asteroid.
Once the whole mass is computed, the trajectory can be determined. In each step, the gravitational influence of each element is considered. This may not be the most

efficient procedure, but it gives accurate results since all elements contribute to the acceleration calculation at every time step. The acceleration exerted by each point mass is given in equation 9.

$$\mathbf{a}_{\text{grav}} = -G \sum_{i=1}^{n} \frac{m_i(\mathbf{r} - \mathbf{r}_i)}{|\mathbf{r} - \mathbf{r}_i|^3} \tag{9}$$

where:

- $\vec{a}_{\text{grav}}$ is the total gravitational acceleration exerted on the spacecraft,
- G is the gravitational constant with a value of, $G = 6.674 \times 10^{-11}\,\text{m}^3\,\text{kg}^{-1}\,\text{s}^{-2}$,
- n is the total number of mass elements,
- m_i is the mass of the i-th tetrahedron element,
- $\vec{r}$ is the position vector of the spacecraft,
- $\vec{r}_i$ is the position vector of the center of mass of the i-th tetrahedron,
- $|\vec{r} - \vec{r}_i|$ is the distance between the spacecraft and the i-th tetrahedron element.

Similarly, to compute the gravitational potential, the value at every point from 1 km above the surface to the surface is computed. This is done using the formula 10

$$V(\mathbf{r}) = -\sum_{i=1}^{N} \frac{G \cdot m_i}{|\mathbf{r} - \mathbf{r}_i|} \tag{10}$$

where:

- $V(\mathbf{r})$ is the gravitational potential at the point $\mathbf{r}$.
- G is the gravitational constant,$G = 6.67 \times 10^{-11}\ \frac{m^3}{kg \cdot s^2}$
- m_i is the mass of the i-th tetrahedral element.
- $\mathbf{r}_i$ is the position vector of the center of mass of the i-th tetrahedral element.
- $|\mathbf{r} - \mathbf{r}_i|$ is the distance between the point of interest $\mathbf{r}$ and the center of mass of the i-the tetrahedral element.

The trajectory of the spacecraft is then simulated by solving the equations of motion, incorporating both the gravitational force and other perturbations such as solar radiation pressure. The motion equation integrated over time is given by equation 11.

$$\ddot{\mathbf{r}} = -\nabla V(\mathbf{r}) + \mathbf{a}_{\text{SRP}} \tag{11}$$

where:

- $\ddot{\vec{r}}$ is the acceleration of the spacecraft,
- $V(\vec{r})$ is the gravitational potential at the position $\vec{r}$ of the spacecraft.
- $\vec{a}_{\text{SRP}}$ is the acceleration due to solar radiation pressure acting on the spacecraft.

This detailed accounting ensures precise modeling of the spacecraft's trajectory as it moves through the asteroid's gravitational field, considering both the micro-variations in the asteroid's density and macro-level influences such as solar radiation. Thus, the trajectories are computed. With the computed trajectories established, we proceed to analyze non-constant density scenarios.

5.3. Non-Constant density Scenarios

Most smaller asteroids are thought to be rubble piles, i.e. debris of different sizes and shapes that have coalesced under the influence of gravity. In the case of Itokawa, [31], an S-type Near-Earth asteroid visited by the Hayabusa mission (JAXA), the asteroid is divided into a higher and lower density lobe. Thus, we have adapted this case to model Apophis, e.g. assuming that the asteroid is divided into two different density regions, see Figure 5. We have chosen 3.2 g/cm^3 and 1.29 g/cm^3 as density values, which are roughly the upper and lower limits for Apophis. In addition, we also looked into a 3-density distribution case for Apophis assuming 3 lobes with respective densities: 3.2 /cm^3, 2.2 /cm^3 and 1.29 g/cm^3. The three lobe density distribution is shown in Figure 7

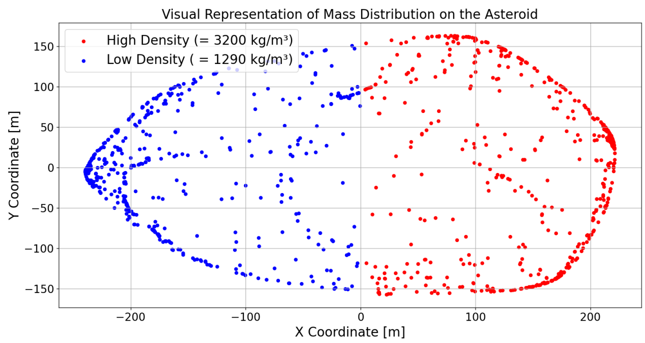

Figure 5: Apophis modeled using the tetrahedral method with 2-density distribution. The blue region represents a density of 1.29 g/cm^3, while the red region corresponds to 3.2 g/cm^3.

The associated trajectories around Apophis with a 2-density distribution are shown in Figure 6. For this 2-density distribution, we obtained a total mass of the asteroid of approx. 4.5 $\cdot 10^{10} kg$ which is within the expected limits defined by [16].

The trajectory of the APOSSUM probe towards Apophis is almost circular, see Figure 6, however the path is slightly perturbed due to the influence of the SRP. Moreover, the center of mass has a greater shift towards the denser lobe than for the 3 density asteroid scenario. This observation indicates that, upon arrival depending on the real density distribution of Apophis, a more thorough investigation of the asteroid's density will be required to determine the most reliable landing trajectory for the APOSSUM probe.

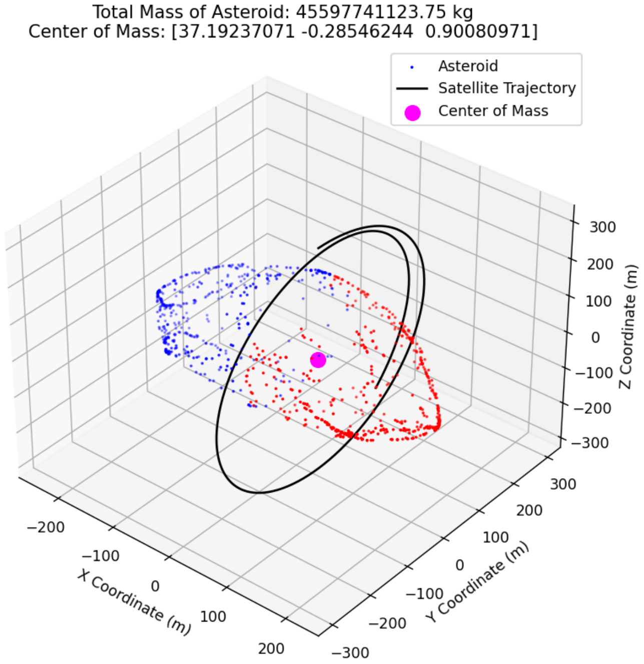

Figure 6: Trajectory simulation around Apophis using the tetrahedral method with two density lobes.

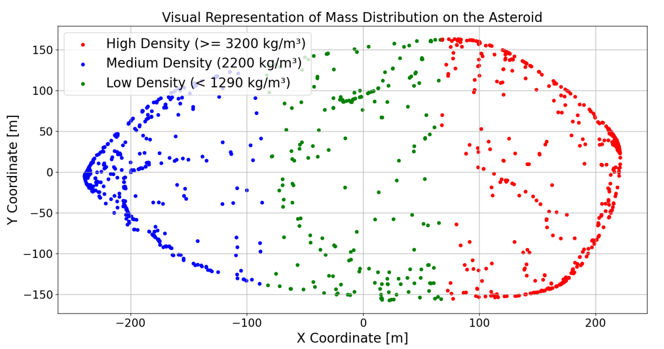

Figure 7: Apophis with three density lobes modeled using the tetrahedral method. The blue region represents a density of 1.29 g/cm^3, the green region 2.2 g/cm^3, and the red region 3.2 g/cm^3.

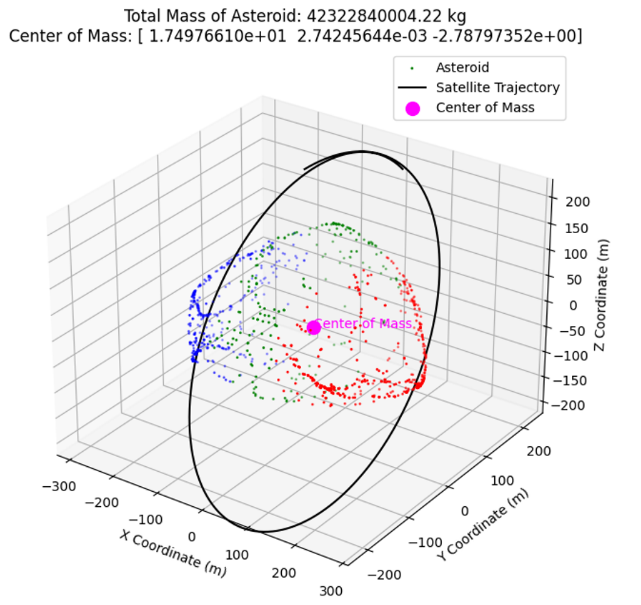

Figure 8: Trajectory path of the APOSSUM lander for the 3-density distribution case of Apophis. The path is influenced by high-density lobes and central mass attraction, showcasing adjustments from gravitational perturbations and solar radiation pressure.

As illustrated in Figure 8, the trajectory is perturbed in such a way that it tends to align toward the center of mass while being influenced simultaneously by the gravitational attraction of the denser lobe. The initial velocity used corresponds to the theoretical one using the mass of the asteroid, calculated using $\sqrt{\frac{GM}{r}}$ [32]. Although the trajectory is close to circular, it is not exactly. This is because, in this scenario, the gravitational perturbation is more complex, and the SRP is also taken into account, as explained in the previous study case.
As explained, the two density scenarios reveal significant differences in the behavior of APOSSUM's trajectory and the position of the center of mass due to the density scenarios. In addition, the orbital period varies between the two cases, since it is dependent on the mass of the asteroid. As shown in the figures, the APOSSUM probe is able to make almost 1.5 rotations in the 2-density lobe scenario and barely one in the other case. This discrepancy is attributed to the initial velocity used, which is proportional to the mass of the asteroid. Since the mass is higher in the first case, the resulting velocity is also higher, leading to a shorter rotation period.

5.4. Controlled landing on Apophis

Once the non-uniform density scenario has been established, control techniques can be applied for landing. Usually, the most efficient maneuver would be computed by trial and error to use the gravitational potential in favor of the spacecraft and so orbit it as it lands in a curved trajectory. Since the APOSSUM probe has to communicate

with RAMSES [11], we have to anticipate a rectilinear trajectory for APOSSUM and therefore we have to look for an optimized control technique.
To achieve a successful landing, 2 control techniques have been tested, including the proportional derivative control (PD) [33] and the bang-bang control [34].
In PD control, the control input is based on both the current error and the rate of change of the error (which is the derivative term). It calculates the desired velocity change using a proportional term and the current velocity, which acts as a derivative term [35].

$$\Delta V = K_p \cdot \mathbf{e}(t) + K_d \cdot \frac{d\mathbf{e}(t)}{dt} \tag{12}$$

where:

- K_p is the proportional gain.
- $\vec{e}(t)$ is the error vector (difference between the target position and the current position).
- K_d is the derivative gain.
- $\frac{d\vec{e}(t)}{dt}$ is the rate of change of the error (difference between the target velocity and the current velocity).

Moreover, it has to be mentioned that for this calculations a maximum ΔV and a minimum one were set. This values were computed using Newton´s equation and the corresponding thrust of the engine used in the spacecraft.

$$\Delta V = \frac{T \cdot \Delta t}{m_{sc}} \tag{13}$$

Several trials were conducted to fine-tune the parameters and optimize the results in every iteration.

Kp	**Kd**	**dt [s]**	ΔV	**Tol.**	**Time [s]**	**Success**
0.005	0.002	12.5 & 1	2.63	2	1635	Success

Table 2: Best trial using PD control with updated gains

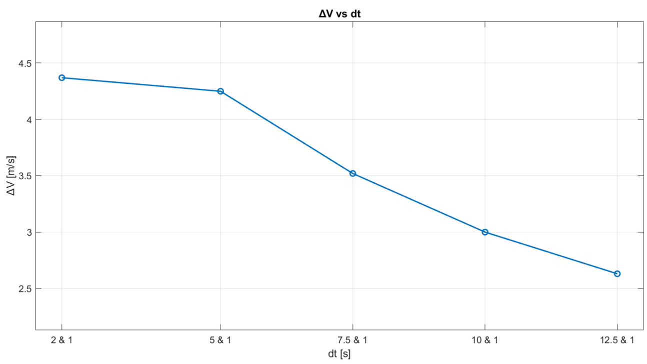

Figure 9: Results using PD control to reduce the time step. The plot compares the total ΔV against the time step between corrections.

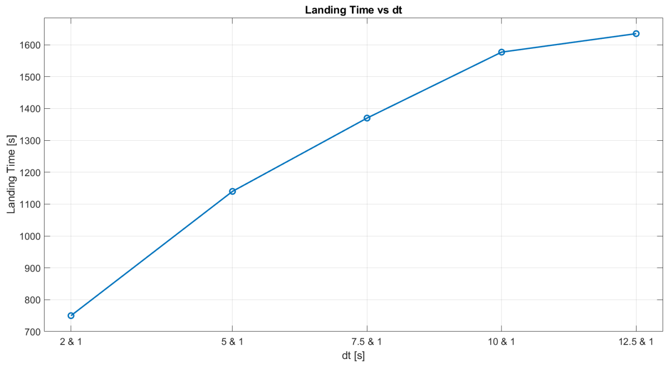

Figure 10: Results using PD control to reduce the time step. The Y-axis shows the landing time in seconds, while the X-axis shows the time step in seconds.

As shown in Table 2, using PD control method, the needed time for the spacecraft to land is 1635 seconds and the ΔV is relatively low. This low value is achieved by doing small increments in velocity along the path, and therefore the needed time rises. Moreover, Figure 9 is shown to have a deeper view of the relationship between the minimum time step at which the algorithm corrects the trajectory, and the ΔV. The 2 values on each position on the x-axis are due to the fact that this technique uses 2 different minimum time step corrections along the path. When the lander is at a height greater than 50 meters the Δt used is the greater value, in this case varies for every trial from 12.5 to 2 s, whereas for closer distances, it is reduced to 1 second. For APOSSUM, this altitude of 50 meters was selected as the transition point to fine control, aligning with Hayabusa2's successful sampling strategy. It provides sufficient time to mitigate gravitational perturbations and ensure a stable touch-and-go operation [36].
Additionally, Figure 9 shows a linear trend where a reduction in time step results in a smaller ΔV. This allows APOSSUM to save more propellant on the way at a time cost, as it can be seen in Figure 10.

On the other hand, Bang bang control technique is a simple on-off control strategy where the control input is switched between its maximum and minimum values of thrust to drive the system towards a desired state. This control technique is often used in the case precise control is not required, and the system can tolerate abrupt changes [37].

$$\mathbf{e}(t) = \text{target} - \text{position} \tag{14}$$

The unit error vector is obtained by normalizing the error vector to get the direction in which the spacecraft needs to move.

$$\Delta V = \begin{cases} \Delta V_{\max} & \text{if } \vec{e}(t) \geq 0 \\ -\Delta V_{\max} & \text{if } \vec{e}(t) < 0 \end{cases} \tag{15}$$

This correctly shows that the change in velocity ΔV is set to ΔV_{max} if the error vector (e(t)) is positive, and

-ΔV_{max} if the error vector is negative. Moreover, one may have noticed the maximum ΔV is the same one as for the PD control technique.

Kp	dt	ΔV	Tol.	Time [s]	Success
-	1	3.94	3	458	Success

Table 3: Best trial using Bang-Bang control

The rotation of the asteroid was also taken into account for these studies. The period used was 30.56 hours, as shown in [38],[39].

When comparing these techniques, both have merits to be suitable; nevertheless, one of them is better for landing than the other.

Although the Bang-bang control algorithm is relatively straightforward to implement and achieves an earlier arrival at the landing site, its reliance on high-thrust impulses results in significantly higher fuel consumption, as shown in 3. On the other hand, Table 3 shows that the landing time is significantly reduced when using Bang-Bang. This is due to the switch between maximum thrust and none. Although this approach reduces time, it does so by increasing the propellant usage. So, it can be noticed that this is a suitable option in case there is a strict time constraint. Nevertheless, since APOSSUM is not driven by a time constraint, it is preferred to save propellant for the return from the asteroid to Earth.

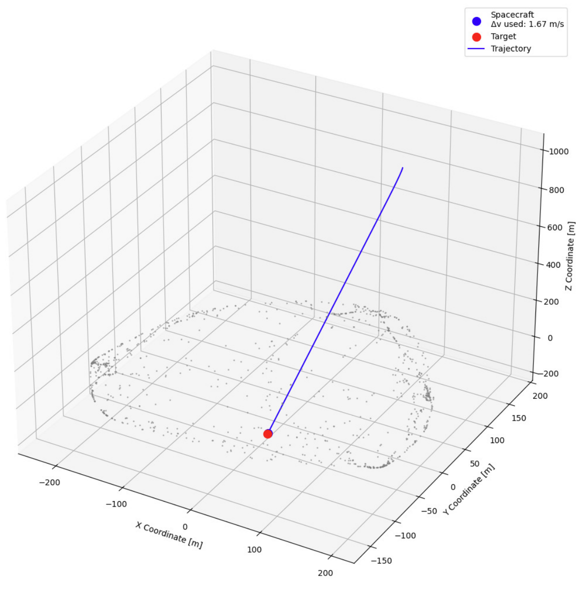

Figure 11: Final trajectory using PD control to land

Figure 11 shows the trajectory of the APOSSUM probe to a target location on the surface of the asteroid. The ΔV is 2.63 m/s as shown in Table 2, the resulting path is almost rectilinear. Furthermore, landing velocity meets the requirements of the GNC subsystem, which specifies a maximum vertical velocity of 0.2 m/s and a maximum lateral velocity of 0.05 m/s to prevent rebound. The spacecraft successfully landed with a vertical velocity of 0.09 m/s and a lateral velocity of 0.05 m/s. The reason behind these requirements comes from the experience of Osiris-Rex [40] and Hayabusa2 [41], the restrictions of the vertical and lateral velocity have been defined during the design process to be 0.2 m/s and 0.05 m/s respectively, very similar to the values used in those missions. This will allow a spring-loaded touchdown of APOSSUM and guarantees that the sampler will not tilt.

5.5. Limitations of the PD Control

Once the PD control technique was chosen based on its suitability for the mission, it became necessary to verify whether this controller can handle a variety of density distributions and conditions. Although the PD controller performs adequately in the three-lobe scenario described above, its limitations need to be accounted for in case this method is not suitable for all configurations.

For the identification of potential limitations, the alternative model from section 5.3 is considered, which describes the 2 density-lobe scenario. That model provides another internal structure of the asteroid, and hence presents another possible environment of the APOSSUM upon arrival. Using the same PD gains and ΔV limits as before, is expected to identify whether the controller would fail the final velocity constraints or needs further adaptation.

Model	V. Vel.	L. Vel	Time [s]	Δv	Success
2-lobe	-0.082	0.057	1327	3.15	No
3-lobe	-0.093	0.036	1635	2.63	Yes

Table 4: Comparison of 2-lobe vs. 3-lobe distributions using the PD controller.

Please note that the velocities of Table 4, are in m/s. As it can be seen, the controller meets the vertical and lateral velocity requirements only in the three-lobe scenario. In the two-lobe case, the larger lateral offset induces a final lateral velocity slightly above 0.05 m/s, thus failing the requirement. These findings indicate that while the PD controller is successful for the three-lobe model, it may require fine-tuning in other density distributions. The next subsection extends these analyses via a Monte Carlo simulation (Section 5.6), focusing primarily on the three-lobe scenario.

5.6. Monte Carlo Simulation

In order to assess the reliability and accuracy of the modelled landing maneuver with the parameters used in the PD control technique and to provide a quantified success rate, a Monte Carlo simulation was performed taking into account relevant uncertainties.

Table 5: Monte Carlo Simulation Parameters

Parameter	Variation	Distribution
Mass (kg)	Uniform	100 ± 10
Area (m^2)	Uniform	0.22 ± 0.05
Position Noise (m)	Gaussian	$\mu = 0$, $\sigma = 0.1$
Velocity Noise (m/s)	Gaussian	$\mu = 0$, $\sigma = 0.01$
Gravitational Model Error (%)	Gaussian	$\mu = 0\%$, $\sigma = 5\%$
SRP Force Noise (%)	Gaussian	$\mu = 0\%$, $\sigma = 2\%$
Density High (kg/m^3)	Uniform	3200 ± 300
Density Mid (kg/m^3)	Uniform	2200 ± 200
Density Low (kg/m^3)	Uniform	1290 ± 100

As summarized in Table 5, the parameters varied during the Monte Carlo simulation were focused on the relevant variables of the system.The mass and cross-sectional area have been varied by 10% and 22% respectively to account for any possible future change. Moreover, some position and velocity noise have been introduced using Gaussian distributions to simulate sensor inaccuracies. Moreover, the simulation also tries to take into account the Gravitational model error and the SRP Force noise for those cases in which some errors in the measurement are made, and the gravitational perturbations from 3rd bodies like Earth, although the influence does not affect, due to the large distance. Finally, the 3 density values are changed in a uniform way to represent material inconsistencies within Apophis.

Using those parameters, a Monte Carlo simulation was done for 5000 cases and APOSSUM achieved a 99.96% success. For a case to be successful, it has to land within the 3 meter location threshold , its terminal velocity has to be below the escape velocity and it has to fulfill the requirements of the vertical and lateral maximum velocities.

It was found that the Average Terminal Velocity Error was 0.10 m/s, with the Maximum Terminal Velocity Error also recorded at 0.10 m/s, demonstrating consistent and minimal velocity deviations across all simulations. The Average Position Error was 0.99 meters, which is well within the predefined distance tolerance limits, further confirming the precision and reliability of the PD controller with timestep variation at 50 m height under varied operational conditions.

6. Phase 3: Return to Earth

Once the samples are collected, the sample phase ends and so the return to Earth starts.

The landing location on Earth is chosen to be Woomera, exemplary landing location for this study, which is the dessert part of Australia (-31º,128º). This location is selected due to its sparse population, which minimizes the risk to human life and property. Moreover, the mission design also considers that the asteroid needed to be on the opposite side of the Earth during the landing in Woomera to ensure undisturbed observation of Apophis by the telescopes. For the departure date from Apophis several dates were considered as candidates, and so several simulations were computed in order to see the best fit.

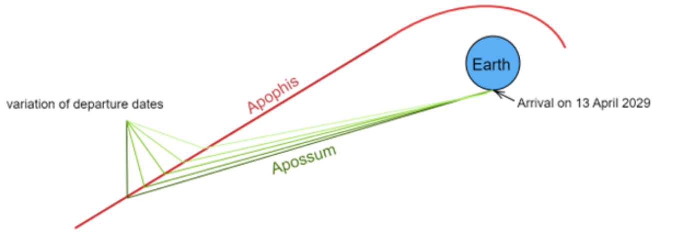

Figure 12: Returning dates

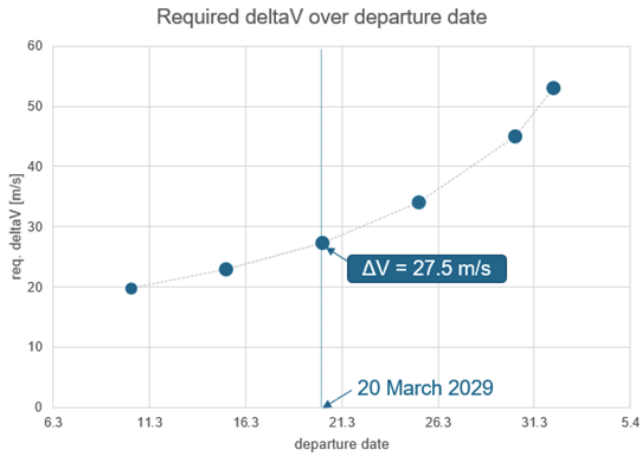

Figure 13: ΔV associated with the respective departure dates

As shown in Figures 12 and 13, the closer the departure date is to the closest encounter of Apophis to Earth, the more ΔV is needed for the return. This is because the trajectory needs a greater correction and acceleration to arrive on the same date. A trade off was made, taking this fact into account along with a requirement of the FPA (Flight path angle) that the APOSSUM probe must have when approaching LEO (20º or less) for the reentry in the atmosphere [42].

By taking these data and requirements into consideration, the departure date was chosen to be 20th March 2029 and the resulting day of arrival on Earth is 13th April 2029, which is the one corresponding to the closest distance of Apophis to Earth [43].

7. Summary and Conclusion

This paper presents a study of the mission scenario of a asteroid sample return mission, APOSSUM, to the asteroid Apophis using ESA's RAMSES spacecraft as carrier. This analysis particularly focused on the controlled landing of the APOSSUM probe assuming that Apophis bulk density is not constant. In contrast to the findings by [14], this paper provides insights in control strategies that can be used to counteract the perturbations that the spacecraft may find during the landing phase in a complex density scenario.

The incorporation of a non-constant density model marks a significant departure from traditional landing analyses, which often assume uniform density distributions. This study highlights the importance of considering density variations in trajectory planning and control design. For future missions, introducing dynamic time steps during trajectory corrections or refining control gains based on local gravitational gradients could further enhance landing precision and fuel efficiency. These findings provide valuable insights for landing missions targeting asteroids with complex internal structures, paving the way for more robust guidance and control systems.

The Key Findings in terms of **Control techniques**: For Phase 1, the "Separation and Approach", it can be done without any control technique using one impulse. For Phase 2, the PD control technique has proved to be a better option for landing since there is no strict time restriction and so, saving ΔV is preferred [44]. Moreover, the trajectory of the bang bang approach will be less stable and straight due to the explained changes between maximum and zero thrust [34]. This means that for a mission with a stronger restriction in time and landing location accuracy, rather than fuel consumption, a Bang-bang control strategy is a more suitable option.

Furthermore, while the PD control method proved highly effective for the APOSSUM mission scenario, it is not without limitations. The need for precise time step tuning and reliance on accurate gravitational models could pose challenges for real-time adaptability to other asteroids. Additionally, it requires computational resources for adaptive time steps and potential overcorrection risks during final descent highlight areas for future optimization. These limitations point to the potential benefits of integrating more advanced control strategies, such as model-predictive control or hybrid approaches, to further enhance robustness and efficiency.

Landing Precision The precision is higher with a PD control as modular thrust is a great advantage when trying to land in a small landing place. This is crucial for missions requiring exact placement of the spacecraft, particularly in regions with challenging topography or when specific scientific objectives require landing in a defined area.

The use of PD and Bang-Bang control for a mission with changing density distributions revealed both limitations and areas for improvement. Without adjustments like varying time steps in PD control, the lander would struggle to achieve precise landings within a 3-meter radius, as gravitational perturbations near denser lobes significantly affect trajectory stability. Bang-Bang control, while faster, consumes more fuel due to its reliance on high-thrust impulses, making it less efficient for fuel-limited missions. Moreover, this control technique needs fine tuning and it is not recommended for these kind of missions

Future missions could benefit from implementing dynamic time steps during trajectory corrections or fine-tuning control gains. These adjustments would allow spacecraft to better handle irregular gravitational environments and improve landing precision, particularly in missions targeting small or highly variable landing areas. Such strategies would enhance robustness and minimize fuel consumption under challenging conditions.

Impact of Density Variations: The study also explored the impact of Apophis's density variations on the spacecraft's trajectory. Changing density distributions were found to cause significant perturbations in the trajectory, which makes it essential to account for these variations in control techniques to ensure a successful landing. The final chosen density distribution is an example that corresponds to the case of a 3 density lobes distribution.

In conclusion, this research provides information on the control techniques to land on an asteroid, showing different scenarios and control techniques for a successful mission. The findings are helpful not only for guidance navigation and control, but also for future mission campaigns that want to explore small celestial bodies, since a similar approach can be used. A similar approach can be adapted for other mission objectives, including those involving targets located further away but still within a few lunar distances from Earth. For instance, the methodologies outlined here could inform missions aiming to land on near-Earth objects (NEOs) or even conduct sample return operations from distant asteroids. For these cases, the approach can be similar by adapting the densities and shape to correspond to the target asteroid. The only significant difference would be in the return phase, as this spacecraft is designed to account for the close proximity of Apophis during its encounter. Other targets may require more time and a higher ΔV.

References

[1] C. W. V. Wolner, 1. a time capsule from the early solar system is en route to earth, Eos (2022). doi:10.1029/2022eo220370.

[2] E. Anders, Pre-biotic organic matter from comets and asteroids, Nature 342 (1989) 255–257. doi:10.1038/342255a0. URL https://doi.org/10.1038/342255a0

[3] H. Yabuta, G. D. Cody, C. Engrand, Y. Kebukawa, Macromolecular organic matter in samples of the asteroid (162173) Ryugu, Science 379 (6634) (2023) eabn9057. arXiv:https://www.science.org/doi/pdf/10.1126/science.abn9057, doi:10.1126/science.abn9057. URL https://www.science.org/doi/abs/10.1126/science.abn9057

[4] Y. Oba, Y. Takano, J. P. Dworkin, Ryugu asteroid sample return provides a natural laboratory for primordial chemical evolution, Nature 14 (2023). doi:10.1038/s41467-023-38518-1. URL https://www.nature.com/articles/s41467-023-38518-1

[5] D. S. Lauretta, H. C. Connolly, J. E. Aebersold, C. M. O. Alexander, R. L. Ballouz, Asteroid (101955) bennu in the laboratory: Properties of the sample collected by osiris-rex, Me-

teoritics & Planetary Science 59 (9) (2024) 2453–2486. doi:10.1111/maps.14227.
URL https://doi.org/10.1111/maps.14227

[6] D. S. Lauretta, H. C. C. Jr, J. E. Aebersold, Asteroid (101955) Bennu in the laboratory: Properties of the sample collected by OSIRIS-REx, Meteoritics & Planetary Science 59 (9) (2024) 2453–2486. doi:10.1111/maps.14227.
URL https://doi.org/10.1111/maps.14227

[7] B. D. Seery, M. Bambacus, R. Leung, K. Greenaugh, F. Raccah, M. Boslough, C. Yang, Near earth object mitigation studies, in: 2016 IEEE Aerospace Conference, IEEE, 2016, pp. 1–12. doi:10.1109/AERO.2016.7500546.

[8] M. E. Banks, Dart mission deflects asteroid in first-of-its-kind test, Physics World 35 (11) (2022) 13i–13i. doi:10.1088/2058-7058/35/11/16.

[9] P. Michel, M. Kueppers, I. Carnelli, H. S. Team, The esa hera mission to the near-earth asteroid binary (65803) didymos: Documentation of the nasa dart impact and full characterization of the asteroid system, Bulletin of the AAS 55 (8) (2023). doi:10.3847/25c2cfeb8a0a2400012fa45f.
URL https://baas.aas.org/pub/2023n8i201p07

[10] A. Buscarino, C. Famoso, L. Fortuna, G. L. Spina, Nasa dart mission: A preliminary mathematical dynamical model and its nonlinear circuit emulation, Nonlinear Engineering 12 (1) (2023) 20220314. doi:10.1515/nleng-2022-0314.
URL https://doi.org/10.1515/nleng-2022-0314

[11] ESA, Introducing ramses, esa's mission to asteroid apophis, https://www.esa.int/Space_Safety/Planetary_Defence/Introducing_Ramses_ESA_s_mission_to_asteroid_Apophis (2024).

[12] M. Hilchenbach, O. J. Stenzel, C. Renggli, A. Nathues, N. Krupp, H. Fischer, T. Kleine, J. Biele, S. Ulamec, J. T. Grundmann, T.-M. Ho, C. Güttler, B. Gundlach, M. Goldmann, N. Schmitz, N. Aksteiner, S. Chand, F. Eichstaedt, O. Eßmann, H. Feiler, T. Firchau, S. Fexer, P. Goldyn, M. Heberhold, V. Hernandez Megia, E. Ksenik, M. Lange, P. Marquardt, F. C. Passenberg, D. Quantius, A. Schneider, F. M. Seibert, M. Siemer, S. Theil, G. Tsakyridis, N. Wendel, T. Wippermann, L. Witte, Snatching a probe of a genuine near-earth asteroid: Fast sample return opportunity in the frame of ramses mission scenario, in: Apophis T-5 Years Workshop, no. #2011 in Apophis T-5 Years, USRA, 2024.
URL https://elib.dlr.de/207006/

[13] T. M. Ho, M. Hilchenbach, J. T. Grundmann, S. Ulamec, J. Biele, F. Dannemann, B. Gundlach, H. Fischer, C. Güttler, M. Grott, T. Kleine, N. Krupp, M. Lange, A. Nathues, D. Quantius, Scientifically strengthening an asteroid mission with small probes on ramses as use case, in: Proceedings of the International Astronautical Congress (IAC), IAC-24, A3, 4A, 10, x85066, International Astronautical Congress (IAC), Milan, Italy, 2024.

[14] D. Scheeres, Proximity operations about apophis through its 2029 earth flyby, arXiv preprint arXiv:2211.10903, available at: https://arxiv.org/abs/2211.10903 (November 2022). doi:10.48550/arXiv.2211.10903.

[15] R. S. Park, R. A. Werner, S. Bhaskaran, Estimating small-body gravity field from shape model and navigation data, Journal of Guidance, Control, and Dynamics 33 (1) (2010) 212–221. doi:10.2514/1.41585.

[16] G. Valvano, O. C. Winter, R. Sfair, R. Machado Oliveira, G. Borderes-Motta, T. S. Moura, APOPHIS – effects of the 2029 Earth's encounter on the surface and nearby dynamics, Monthly Notices of the Royal Astronomical Society 510 (1) (2021) 95–109. doi:10.1093/mnras/stab3299.

[17] Y. Weidong, L. Shu, Y. Yu, Y. Gao, Use of tetrahedral finite element method for computing the gravitation of irregular-shaped asteroid, IOP Conference Series: Materials Science and Engineering 608 (2019) 012043. doi:10.1088/1757-899X/608/1/012043.

[18] MathWorks, Matlab - the language of technical computing, accessed: 2024-11-26 (2024).
URL https://de.mathworks.com/products/matlab.html

[19] L.-L. Yu, J. Ji, W.-H. Ip, Surface thermophysical properties investigation of the potentially hazardous asteroid (99942) apophis, Research in Astronomy and Astrophysics 17 (03 2017). doi:10.1088/1674-4527/17/7/70.

[20] P. Pravec, P. Scheirich, J. Ďurech, J. Pollock, P. Kušnirák, The tumbling spin state of (99942) apophis, Icarus 233 (2014) 48–60. doi:10.1016/j.icarus.2014.01.026.
URL https://doi.org/10.1016/j.icarus.2014.01.026

[21] G. Frieger, Asteroid (99942) apophis 3d model, accessed: 2024-12-02 (2021).
URL https://3d-asteroids.space/asteroids/99942-Apophis

[22] MeshLab, Meshlab, accessed: 2024-12-02 (2024).
URL https://www.meshlab.net/

[23] M. Brozović, L. A. M. Benner, J. G. McMichael, J. D. Giorgini, P. Pravec, P. Scheirich, C. Magri, M. W. Busch, J. S. Jao, C. G. Lee, L. G. Snedeker, M. A. Silva, M. A. Slade, B. Semenov, M. C. Nolan, P. A. Taylor, E. S. Howell, K. J. Lawrence, Goldstone and arecibo radar observations of (99942) apophis in 2012–2013, Icarus 300 (2018) 115–128. doi:10.1016/j.icarus.2017.08.032.
URL http://dx.doi.org/10.1016/j.icarus.2017.08.032

[24] S. Goossens, D. E. Smith, Gravity degree–depth relationship using point mass spherical harmonics, Geophysical Journal International 233 (3) (2023) 1878–1889. doi:10.1093/gji/ggad036.
URL https://doi.org/10.1093/gji/ggad036

[25] J. R. Taylor, Classical Mechanics, University Science Books, Sausalito, CA, 2005.

[26] S. J. Mohammed, M. A. Mohammed, Runge-kutta numerical method for solving nonlinear influenza model (11 2021). doi:10.1088/1742-6596/1879/3/032040.

[27] D. A. Vallado, Fundamentals of astrodynamics and applications, in: 4th ICATT, Madrid, Spain, Tutorial Lectures, European Space Agency (ESA), 2010.
URL https://trajectory.estec.esa.int/Astro/4rth-astro-workshop-presentations/ICATT-2010-Tutorial-ASTRODYNAMICS.pdf

[28] V. Pesce, A. Colagrossi, S. Silvestrini, Modern Spacecraft Guidance, Navigation, and Control, Elsevier, 2023. doi:10.1016/C2020-0-03563-2.

[29] Y. Takahasi, Spherical harmonic potentials within the brillouin sphere, in: AIAA/AAS Astrodynamics Specialist Conference, American Institute of Aeronautics and Astronautics (AIAA), 2014. doi:10.2514/6.2014-4302.

[30] K. F. Riley, M. P. Hobson, S. J. Bence, Mathematical Methods for Physics and Engineering, 3rd Edition, Cambridge University Press, 2006.

[31] S. C. Lowry, P. R. Weissman, S. R. Duddy, B. Rozitis, A. Fitzsimmons, S. F. Green, M. D. Hicks, C. Snodgrass, S. D. Wolters, S. R. Chesley, J. Pittichová, P. van Oers, 5. the internal structure of asteroid (25143) itokawa as revealed by detection of yorp spin-up, Astronomy and Astrophysics (2014). doi:10.1051/0004-6361/201322602.

[32] D. R. Brooks, An introduction to orbit dynamics and its application to satellite-based earth monitoring systems, Tech. Rep. NASA-TM-X-73605, NASA (1977).
URL https://ntrs.nasa.gov/api/citations/19780004170/downloads/19780004170.pdf

[33] R. Borase, D. Maghade, n. c. s. a. Sondkar, A review of pid control, tuning methods and applications, SpringerLink 9 (2020). doi:10.1007/s40435-020-00665-4.

[34] K. Wang, Z. Chen, Z. Wei, F. Lu, J. Li, A new smoothing technique for bang-bang optimal control problems, in: AIAA Science and Technology Forum and Exposition (SciTech), 2023. doi:10.2514/6.2024-0727.

[35] Y. Xie, Y. Lei, J. Guo, B. Meng, Spacecraft Attitude Control, Springer Singapore, Singapore, 2022, pp. 263–370. doi:10.1007/978-981-33-6448-6_6.
URL https://doi.org/10.1007/978-981-33-6448-6_6

[36] H. Sawada, R. Okazaki, S. Tachibana, et al., Hayabusa2 sampler: Collection of asteroidal surface material, Space Science

Reviews 208 (2017) 81–106. doi:10.1007/s11214-017-0338-8. URL https://doi.org/10.1007/s11214-017-0338-8

[37] Wikipedia, Bang–bang control, accessed on 2024-06-27 (2024). URL https://en.wikipedia.org/wiki/Bang%E2%80%93bang_control

[38] Souchay, J., Lhotka, C., Heron, G., Hervé, Y., Puente, V., Folgueira Lopez, M., Changes of spin axis and rate of the asteroid (99942) apophis during the 2029 close encounter with earth: A constrained model, A&A 617 (2018) A74. doi:10.1051/0004-6361/201832914.

[39] S. Wagner, D. Zimmerman, B. Wie, Preliminary design of a crewed mission to asteroid apophis in 2029-2036, in: AIAA Guidance, Navigation, and Control Conference, 2010. doi:10.2514/6.2010-8374.

[40] K. Berry, P. Antreasian, M. C. Moreau, A. May, B. Sutter, Osiris-rex touch-and-go (tag) navigation performance, in: 38th Annual AAS Guidance and Control Conference, American Astronautical Society, Breckenridge, Colorado, 2015, aAS 15-125.

[41] S. Kikuchi, T. Saiki, Y. Takei, F. Terui, N. Ogawa, Y. Mimasu, G. Ono, K. Yoshikawa, H. Sawada, H. Takeuchi, H. Ikeda, A. Fujii, S. Sugita, T. Morota, M. Yamada, R. Honda, Y. Yokota, N. Sakatani, S. Kameda, T. Kouyama, N. Hirata, N. Hirata, K. Shirai, K. Kitazato, S. Nakazawa, M. Yoshikawa, S. Tanaka, K. Wada, S. ichiro Watanabe, Y. Tsuda, Hayabusa2 pinpoint touchdown near the artificial crater on ryugu: Trajectory design and guidance performance, Advances in Space Research 68 (8) (2021) 3093–3140. doi:https://doi.org/10.1016/j.asr.2021.07.031.
URL https://www.sciencedirect.com/science/article/pii/S0273117721006037

[42] K. Lakshmi, P. Priyadarshi, Multi-disciplinary Analysis of a Reentry Vehicle, Springer, 2020, pp. 19–31. doi:10.1007/978-981-15-5432-2_2.

[43] S. Ershkov, D. Leshchenko, Revisiting apophis 2029 approach to earth (staying on shoulders of nasa's experts) or can we be sure in almost ricocheting fly-by of apophis on 13 of april 2029 near the earth?, Journal of Space Safety Engineering 9 (3) (2022) 363–374. doi:https://doi.org/10.1016/j.jsse.2022.05.007.
URL https://www.sciencedirect.com/science/article/pii/S2468896722000453

[44] M. Golestani, K. A. Alattas, S. U. Din, F. F. M. El-Sousy, S. Mobayen, A. Fekih, A low-complexity pd-like attitude control for spacecraft with full-state constraints, IEEE Access 10 (2022) 30707–30715. doi:10.1109/ACCESS.2022.3159480.